Journal of Solid State Electrochemistry
https://doi.org/10.1007/s10008-023-05639-y

ORIGINAL PAPER

Synthesis of nitrogen-doped reduced graphene oxide as counter electrode material for dye-sensitized solar cells

Fahad A. Alharthi[1] · **Imran Hasan**[1]

Received: 23 June 2023 / Revised: 29 July 2023 / Accepted: 9 August 2023

Abstract

Dye-sensitized solar cells (DSSCs) are the most promising photovoltaic technology compared to other third-generation solar cells in terms of stability and cost-effectiveness. DSSCs involve the use of platinum-modified conductive glass substrate such as fluorine-doped tin oxide (FTO) as counter electrode material. Thus, to further reduce the cost of DSSCs, it is required to develop the Pt-free materials and use them as cost-effective counter electrode material for DSSC applications. In the present work, we have fabricated a nitrogen-doped reduced graphene oxide (N-rGO)-coated FTO glass substrates and employed it as counter electrode for DSSCs. The N-rGO/FTO counter electrode exhibited excellent electrocatalytic activity to catalyze the redox reaction. The N-rGO/FTO counter electrode-based DSSCs showed good efficiency of 6.7%. This shows that N-rGO/FTO may be a potential candidate for its use as counter electrode for the construction of DSSCs.

Keywords Nitrogen-doped rGO · Counter electrode · Redox · Dye-sensitized solar cells

Introduction

In the present world, energy consumption has been dramatically increased due to the rapid growth in the global population [1]. Energy crisis may be a major challenge for the scientific community which needs immediate attention [2–4]. The rise in energy costs and the heightened focus on global warming have spurred the development of economically feasible alternatives to fossil fuels [5–7]. In the past few decades, various energy-related technologies have been developed to overcome the issue of energy crisis [8–10]. Renewable energy resources, particularly solar energy, have been proven as the most efficient sources, which has the potential to overcome the issues of energy crisis. Solar energy is a never-ending resource which is available in huge amounts [11–14]. The Earth receives a massive amount of radiation, approximately 120,000 terawatts (TW), from the sun, making it the largest and cleanest energy source available [15]. However, despite this abundance, solar cells currently only generate around 5 gigawatts (GW) of power [16]. The main reason for this is that the cost of solar energy, based on existing technologies, is not competitive with that of fossil fuels [17]. Therefore, it is required to convert solar energy by employing photovoltaic technology [18]. Silicon-based photovoltaic cells, which are the first-generation solar cells, dominate the solar cell market due to their high efficiency [19].

However, they have a disadvantage in that they require a thick active layer to convert solar energy due to their indirect optical band gaps [20]. This leads to an expensive fabrication processes for large area materials. The second generation of photovoltaic (PV) materials aimed to address this issue by depositing thin films, which reduced fabrication costs [21]. Nevertheless, both first- and second-generation devices face similar limitations in performance. They experience "red losses" where photons with energies below the device's band gap cannot be absorbed, and "blue losses" where photons with energies above the band gap lose their excess energy as heat [22]. The third generation of PVs represents the forefront of solar technologies. These devices are designed to surpass the limitations of single-junction devices, offering both high efficiency and low production costs. They are considered the cutting-edge solution in the quest for more advanced solar power. In this context, various photovoltaic technology such as perovskite solar cells,

✉ Imran Hasan
iabdulateef@ksu.edu.sa

Fahad A. Alharthi
fharthi@ksu.edu.sa

[1] Department of Chemistry, College of Science, King Saud University, Riyadh 11451, Kingdom of Saudi Arabia

Published online: 21 August 2023

dye-sensitized solar cells (DSSCs) [23], polymer solar cells [24], organic solar cells [25, 26], and quantum dot solar cells [27, 28] have been developed. Perovskite solar cells have shown excellent performance but the use of toxic lead and poor stability in air restricts their commercialization [29, 30]. In contrast, DSSCs are highly stable compared to the perovskite solar cells and showed good performance [31]. DSSCs comprised various components such as photoanode, dye molecules, redox electrolyte, and counter electrode [32]. The counter electrode consists of platinum-coated fluorine-doped tin oxide (Pt/FTO) which is an expensive and precious metal [33]. Thus, it is very significant to develop the Pt-free counter electrode for the fabrication of cost-effective DSSCs. Due to their high electronic conductivity, resistance to corrosion from I_2, strong reactivity in triiodide reduction, and affordability, carbonaceous materials are highly appealing as potential substitutes for platinum [34, 35]. In the previous studies, various carbon-based materials, including multi-walled carbon nanotubes (MWCNTs) [36], activated carbon [37], single-walled carbon nanotubes (SWCNTs) [38], graphite, and double-walled carbon nanotubes (DWCNTs) [39] have been explored as counter electrode materials for DSSC applications.

Recently, graphene, an intriguing two-dimensional material consisting of a single-layer hexagonal lattice of carbon atoms, has gained considerable attention in the field of condensed-matter physics [40–42]. Graphene exhibits a wide range of exceptional characteristics. It can handle current densities that are six orders of magnitude higher than copper and showcases outstanding thermal conductivity, optical transparency, durability, and rigidity [43]. Additionally, it is impermeable to gases and demonstrates remarkable electronic transport properties at the individual level. While graphene has been extensively studied from a theoretical perspective, its practical application in novel devices has only recently begun [44]. Transparent conductive films [45], organic photovoltaic cells [46], field-effect transistor devices [47], and highly-sensitive sensors [48] are among the various areas where graphene has been utilized. In addition to its unique single-atom thickness, graphene's high hole-transport mobility, extensive specific surface area, and resistance to oxygen and water vapor make it an exceedingly promising material for photovoltaic applications. Studies have shown that the edge plane sites of graphene exhibit faster electron-transfer kinetics compared to the basal plane sites, suggesting that graphene may possess superior electrocatalytic properties compared to carbon nanotubes (CNTs) [49].

In this study, we have fabricated nitrogen-doped reduced graphene oxide (N-rGO)-coated FTO glass substrates for their applications in DSSCs. The fabricated N-rGO/FTO substrate exhibits good electrocatalytic properties, and the constructed DSSCs show decent efficiency. The annealing temperature for counter electrode preparation has been optimized. We propose the role of N-rGO as a promising counter electrode material for DSSC applications.

Materials and methods

Chemicals

N-719 (Di-tetrabutylammonium cis-bis(isothiocyanato) bis(2,2(2,2(2,2 s ountedicarboxylato)ruthenium(II)) dye was bought from Solaronix. Iodine and lithium iodide, guanidine thiocyanate, tert-butyl pyridine, acetonitrile, graphite powder, potassium permanganate ($KMnO_4$), 1-methyl-3-propylimidazolium iodide (MPII), and all solvents were purchased from Merck and Alfa-Aesar.

Synthesis of N-rGO

In the first steps, graphene oxide (GO) prepared was reported elsewhere [50]. Hummer's method, with slight modifications, was employed to generate GO in the initial phase. To illustrate the procedure, a solution containing 23.5 mL of H_2SO_4, 1.10 g of graphite flakes, and 0.55 g of $NaNO_3$ was prepared and allowed to sit at room temperature (RT) for 30 min. To regulate the exothermic reaction, ice was used to maintain the temperature below 18–20 °C, while 3.50 g of $KMnO_4$ was gradually added and stirred continuously overnight at RT. Subsequently, 65 mL of DI water and 1.6 g of $KMnO_4$ were gently introduced to the mixture, followed by another 15 h of stirring at RT. After the completion of the reaction, the mixture was allowed to cool, and 550 mL of DI water and 7.5 mL of 30% H_2O_2 were added. The resulting mixture underwent a brief wash with 1 M HCl, followed by multiple rinses with water. The final product was obtained by washing the resulting mixture with additional DI water and drying it at 45 °C for 12 h. To prepare the N-rGO, 200 mg of GO was dispersed in DI water, and an appropriate amount of melamine was added in the GO dispersion. This reaction solution was transferred to the Teflon reactor and sealed. Furthermore, this autoclave system was heated at 200 °C for 6 h. Finally, the obtained product was washed with ethanol and DI water and dried at 50 °C overnight.

Apparatus

In this research, a range of techniques were employed to meticulously investigate and evaluate the prepared materials. The powder x-ray diffraction (PXRD) patterns of the prepared samples were collected on a Rigaku, Japan, RINT 2500 V x-ray diffractometer (Cu-Kα irradiation; $\lambda = 1.5406$ Å). The morphology of the prepared samples was checked using Supra 55 Zeiss field emission–scanning electron microscope (FE-SEM). Furthermore, the Raman

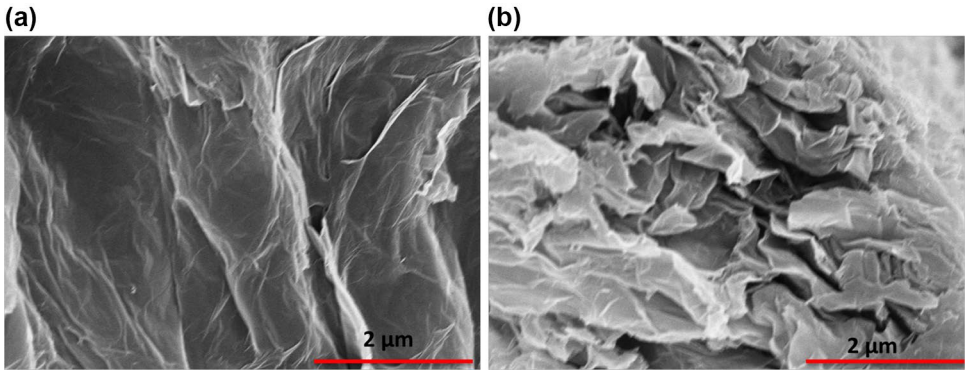

Fig. 1 FE-SEM pictures of GO (**a**) and N-rGO (**b**)

spectrum of the samples was collected on a Raman spectroscope (Bruker Senterra R200-L). The x-ray photoelectron spectroscopic (XPS) results were collected on a Thermo-Scientific instrument. Photocurrent density versus voltage curve were recorded under 1 sun conditions (AM 1.5 solar; 100 mWcm^{-2}) on a solar simulator.

Fabrication of N-rGO/FTO-based DSSCs

The synthesized N-rGO was grounded in terpineol solution (5 wt% of ethyl cellulose). This prepared paste was coated on to the FTO by screen printing and heated at 400 °C for 20 min. This prepared electrode has been used as a counter electrode. On the other side, titanium dioxide (TiO_2) paste was subsequently screen printed onto the FTO substrate and sintered at 500 °C for 30 min. Furthermore, these prepared TiO_2 films were immersed into the dye solution (0.5 mM N719 in tert-butyl alcohol and acetonitrile (ratio = 1:1) at RT for 24 h. The cell holder associated with clamps was used to press the FTO/TiO_2/N719 and N-rGO/FTO electrodes. A drop of liquid electrolyte solution (1 M MPII, 0.05 M I_2, 0.5 M guanidine thiocyanate, and 0.5 M tert-butylpyridine in acetonitrile) was introduced between the photoanode and counter electrodes. Surlyn polymer foil was used as a spacer by introducing surlyn between photoanode and the counter electrode to overcome the issue of short-circuit.

Results and discussion

Characterization

Surface structural properties of the prepared GO and N-rGO were characterized by FE-SEM. The FE-SEM image of the as-obtained GO has been presented in Fig. 1a. The obtained FE-SEM investigations show the characteristic sheet-like surface of the as-prepared GO. Furthermore, we have also examined the surface morphological property of the as-obtained N-rGO. The obtained results are presented in Fig. 1b. The FE-SEM results show that N-rGO has a sheet-like surface with the appearance of wrinkles. The cross-sectional SEM image of the N-rGO has been presented in Fig. S1. These obtained FE-SEM results of the GO and N-rGO are well-matched with the previous reports [51].

After careful FE-SEM investigations, PXRD analysis was also conducted to check the formation, phase purity, and crystalline nature of the as-prepared GO and N-rGO. The obtained PXRD patterns of the N-rGO and GO have been presented in Fig. 2. The as-obtained GO exhibits a diffraction peak around 9.06° which suggests the presence of (001) diffraction plane (Fig. 2). This obtained PXRD pattern confirms the formation of GO and is consistent with the reported literature [50]. The PXRD of N-rGO exhibits the appearance of a new diffraction peak at 2θ value of 23.29°. This diffraction peak indicated the presence of (002) diffraction plane. However, the diffraction peak at 9.06° disappear, which confirmed the conversion of GO to N-rGO and was consistent with previous studies [51].

Raman spectroscopy is an exceptionally straightforward and nondestructive method used to analyze the composition

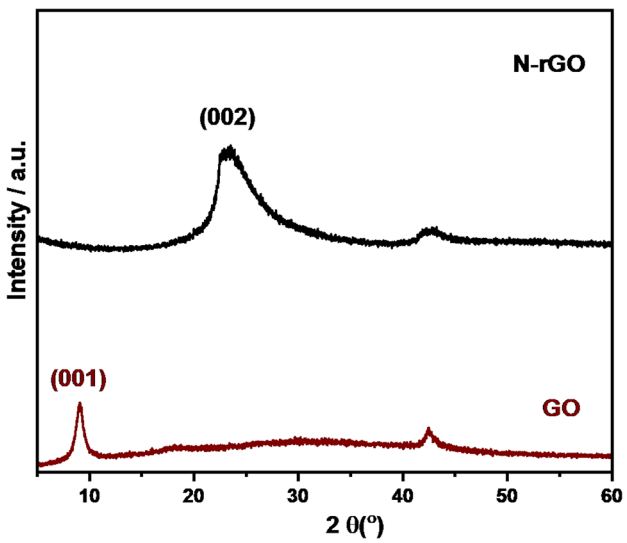

Fig. 2 PXRD of GO and N-rGO

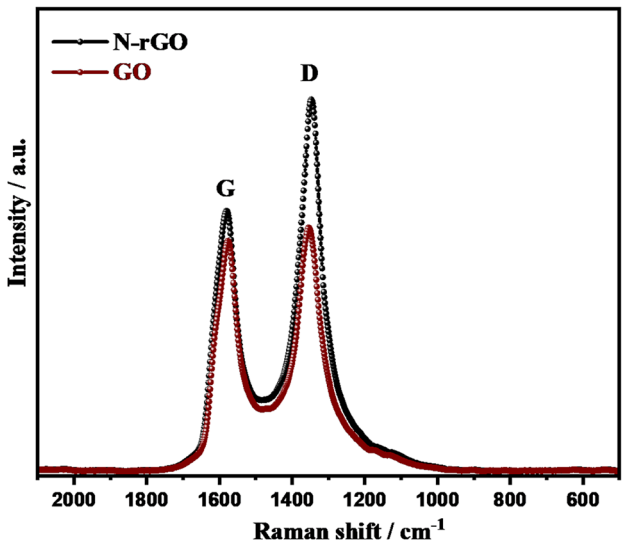

Fig. 3 Raman spectra of GO and N-rGO

and integrity of carbon-based materials. Its primary purpose is to identify defects, as well as distinguish between ordered and disordered structures, and ascertain the layering in materials such as GO and N-RGO. Thus, Raman spectroscopic investigations were performed to further characterize the as-prepared GO and N-rGO. The obtained Raman spectra of GO and N-rGO are provided in Fig. 3. The Raman spectrum of GO showed two prominent peaks, which corresponded to the D and G bands of the prepared GO. The I_D/I_G ratio for GO was found to be 1.06. The Raman spectrum of N-rGO also shows peaks for the D and G bands. The I_D/I_G ratio for N-rGO was found to be 1.42. These observations and results match the previous studies [51].

The XPS method was further performed to study the elemental composition of the prepared N-rGO. Melamine which is known as a nitrogen-rich compound has been used to the GO dispersion. Melamine contains three amino groups ($-NH_2$), which serve as the nitrogen source for doping-reduced graphene oxide. Thus, the presence of N was further confirmed by using XPS. The collected XPS survey scan of N-rGO has been presented in Fig. 4a. The survey spectrum reveals the appearance of C1s, N1s, and O1s. This confirms the presence of N-atom in the prepared N-rGO. The high-resolution N1s scan of N-rGO is shown in Fig. 4b. The obtained N1s spectrum has been fitted which shows the appearance of three peaks at binding energy value of 402.44, 401.2, and 400.2 eV. The peak at 400.2 eV indicated the presence of pyrrole-like nitrogen which contributed to the p-conjugated system with a pair of p-electrons in rGO layers. The substitution of carbon atoms by nitrogen atoms resulted in the appearance of two peaks at 401.2 and 402.44 eV, which can be assigned to the graphitic nitrogen. Figure 4c shows the C1s scan of N-rGO and the fitted peaks show the binding energy of 284.9, 285.5, and 286.3 eV. These three peaks can be assigned to the $sp^2-C=C$, $N-sp^2-C$, and, $N-sp^3-C$, respectively (Fig. 4c). The above results are in agreement with published literature [51].

Photovoltaic studies

Before the fabrication of DSSCs, we examined the electrocatalytic activity of the N-rGO for redox reaction. Cyclic voltammetry (CV) has been used to study the electrocatalytic activity of the N-rGO-coated counter electrode for redox reaction. The CV responses of the N-rGO counter electrode were collected in a redox electrolyte system as discussed above. The obtained CV results have been provided in Fig. 5. The counter electrode serves the purpose of aiding the transformation of I_3^- into I^- at the boundary between the counter electrode and the electrolyte by collecting the electrons generated by the external circuit. The CV of the GO was also obtained under similar conditions, which is presented in Fig. S2. The CV of GO exhibited poor electrocatalytic response. The observations indicated that N-rGO

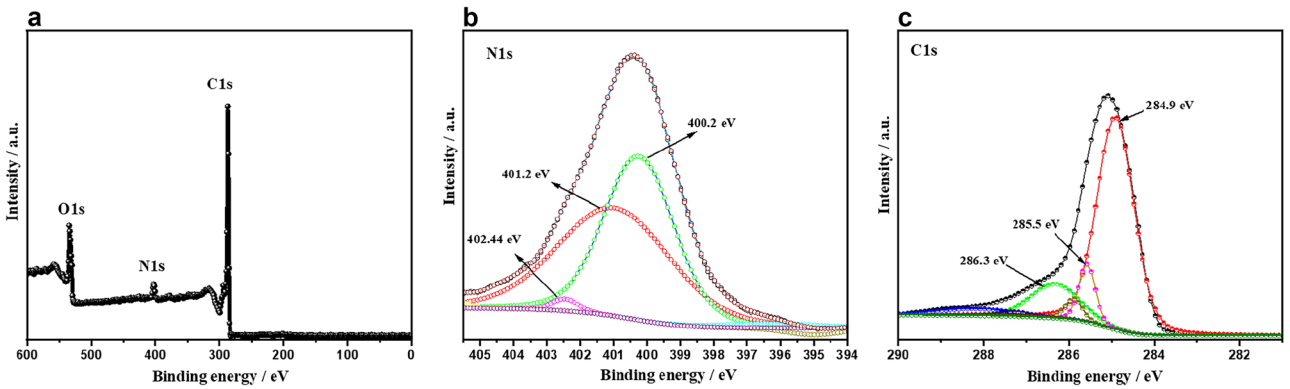

Fig. 4 XPS survey spectrum of **a** N-rGO. N1s (**b**) and C1s (**c**) XPS scan of N-rGO

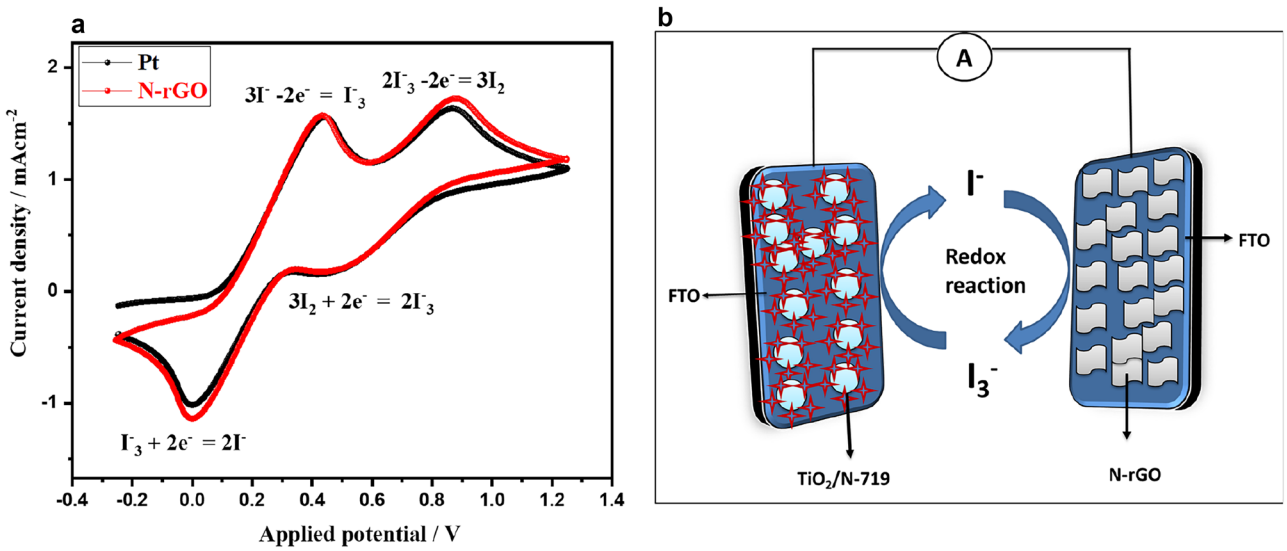

Fig. 5 CV graphs of **a** N-rGO and Pt counter electrodes in iodine redox electrolyte at scan rate = 100 mV/s. Schematic graph of DSSCs (**b**)

has good electrocatalytic activity which is comparable with Pt counter electrode as shown in Fig. 5. The CV response shows the appearance of 2 pairs of oxidation–reduction peaks which can be described below,

$$I_3^- + 2e^- \longleftrightarrow 3I^- \quad \ldots\ldots..$$

$$3I_2 + 2e^- \longleftrightarrow 2I_3^- \quad \ldots\ldots..$$

The above CV results demonstrate the role of N-rGO as a suitable counter electrode material. Hence, we have further fabricated N-rGO-based DSSCs. After physiochemical and electrocatalytic investigations, we have fabricated DSSCs by employing N-rGO as a counter electrode material. The schematic picture of fabricated DSSCs has been depicted in Fig. 5b.

Moreover, the photovoltaic efficiency of N-rGO-based DSSCs was assessed by acquiring their current density-voltage (J-V) curves under standard sunlight conditions, equivalent to 1 sun intensity. Figure 6a displays the J-V graph of N-rGO counter electrode–based DSSCs. The results indicate that N-rGO counter electrode-based DSSCs achieved an intriguing Voc of 0.76 V. Additionally, a PCE of 6.74% was obtained for N-rGO counter electrode-based DSSCs. In order to examine the impact of N-rGO, we have also fabricated DSSCs using Pt as a counter electrode. Figure 6a exhibits the J-V graph of Pt counter electrode-based DSSCs. The findings demonstrate that these DSSCs with Pt counter electrodes attained a noteworthy Voc of 0.71 V. Furthermore, a PCE of 6.85% was achieved for DSSCs utilizing Pt counter electrodes. The photovoltaic parameters of Pt and N-rGO counter electrode-based DSSCs are summarized in Fig. 6b. Figure 6b shows that performance of N-rGO counter electrode-based DSSCs is pretty reasonable compared to the Pt-based DSSCs. This reveals that N-rGO may be used as a cost-effective Pt-free counter electrode material.

The above N-rGO counter electrode-based DSSCs involve the sintering temperature of 400 °C. The sintering temperature for counter electrode plays a significant role and greatly influences the performance of DSSCs. Thus, we have optimized the sintering temperature and obtained PCE with respect to the sintering temperature, as presented in Fig. 6c. The observed results show that 400 °C is the most suitable temperature for the fabrication of N-rGO-based DSSCs with improved power conversion efficiency. This may be due to the better charge transportation or electrical conductivity of the N-rGO-based counter electrode (annealed at 400 °C). The electrochemical impedance spectroscopy (EIS) was used to examine the effect of annealing temperature on the efficiency of the fabricated DSSCs. The Nyquist plots of Pt and N-rGO (annealed at 400 °C) are shown in Fig. S3a. Charge transfer resistances (rct) of 56.7 and 85.1 Ω were observed for Pt and N-rGO- (annealed at 400 °C) based DSSCs, respectively (Fig. S3a). The Nyquist plots of N-rGO (annealed at 250–450 ºC) are shown in Fig. S3b. The rct value of 102.2, 96.5, 91.3, 85.1, and 92.4 Ω were observed for N-rGO-based counter electrode annealed at 250, 300, 350, 400, 450 °C, respectively. Therefore, it is clear that N-rGO- (annealed at 400 ºC) based DSSCs exhibited improved performance.

The stability of the DSSCs is also an important characteristic; therefore, we have checked the stability of the Pt and N-rGO- (annealed at 400 ºC) based DSSCs at different time.

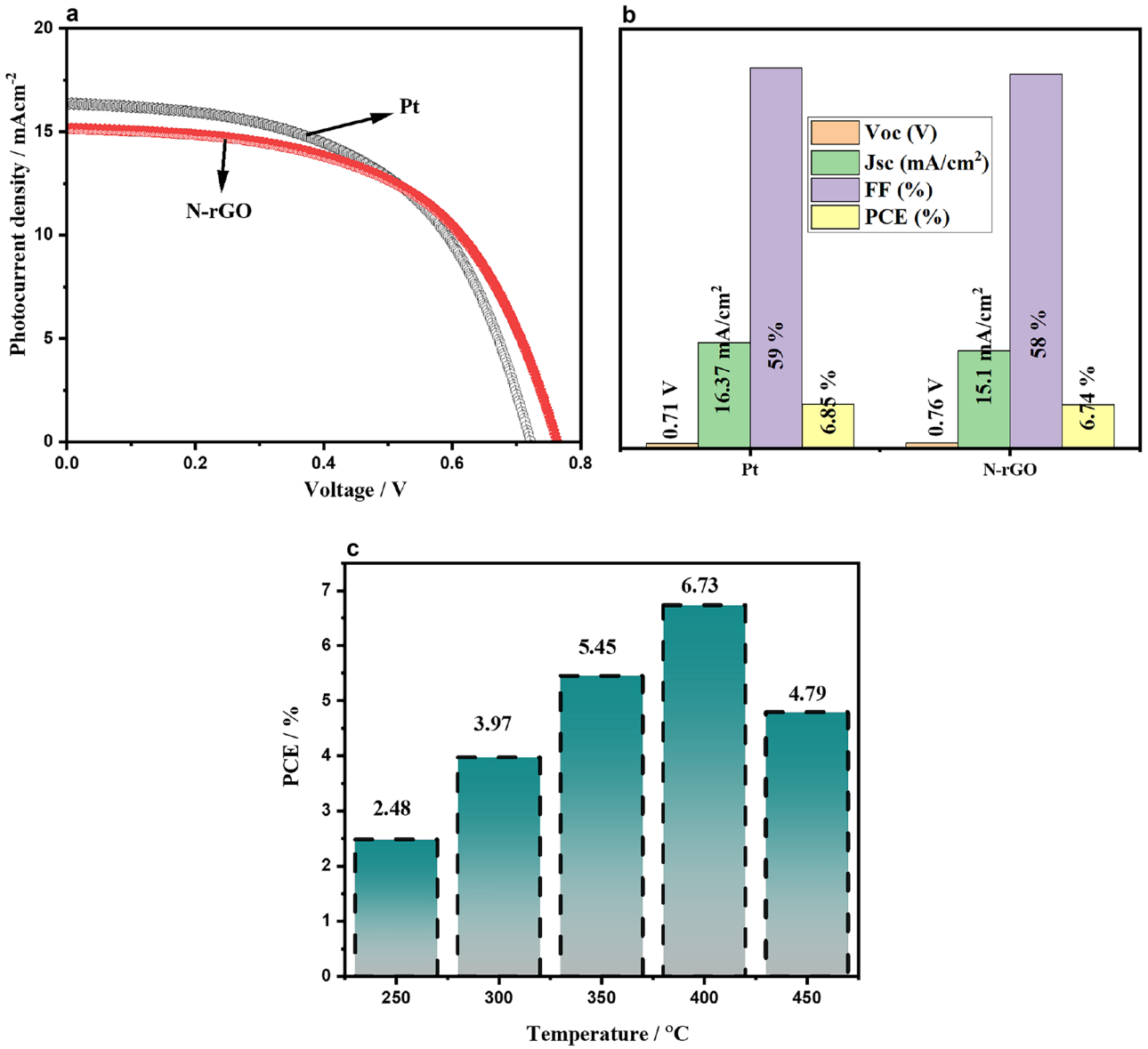

Fig. 6 J-V (**a**) and J-V parameters (**b**) of N-rGO and Pt based DSSCs. PCE graph (**c**) with respect to temperature

Table 1 Comparison of photovoltaic parameters obtained for N-rGO-based DSSCs with previous studies

Counter electrodes	Jsc (mA/cm^2)	Voc (V)	FF (%)	PCE (%)	References
Graphene	16.14	0.68	40.43	4.44	[43]
Graphene/PANI	13.28	0.68	67	6.09	[52]
Graphene/PEDOT	12.60	0.77	63	6.26	[53]
Graphene/PEDOT-PSS	12.96	0.72	48	4.50	[54]
Graphene/MWNTs	5.60	0.76	70	3.0	[55]
Graphene/CNTs	12.86	0.78	61	6.17	[56]
Graphene/$Ni_{12}P_5$	12.86	0.74	61	5.70	[57]
Graphene	12.88	0.70	52	4.70	[58]
N-rGO	10.5	0.72	71	5.4	[59]
N-rGO	15.19	0.68	59	6.12	[60]
N-doped graphene foam	15.84	0.77	58	7.07	[61]
N-rGO	15.1	0.76	58	6.74	**This work**

The obtained PCE are summarized in Fig. S4. It can be seen that N-rGO- (annealed at 400 ºC) based DSSCs retained good PCE after 96 h.

In the previous years, many counter electrode materials have been employed to replace the Pt-based counter electrodes. In this connection, various Pt-free counter electrode materials have been reported as summarized in Table 1. Our obtained performance is reasonable compared to the previous reports as shown in Table 1.

Conclusions

In conclusion, N-rGO has been prepared via hydrothermal method using melamine as the nitrogen source. Furthermore, FTO glass substrate was coated with as-prepared N-rGO and heated at 400 °C. The N-rGO/FTO demonstrated decent electrocatalytic properties. This fabricated electrode (N-rGO/FTO) was employed as a counter electrode for DSSCs. The N-rGO/FTO-based fabricated DSSCs exhibited good photovoltaic performance in terms of power conversion efficiency. The improved power conversion efficiency of 6.74% has been obtained. This obtained power conversion efficiency was found to be comparable with Pt counter electrode-based DSSCs. This work proposed the role of N-rGO/FTO as a promising counter electrode for DSSC applications.

Supplementary Information The online version contains supplementary material available at https://doi.org/10.1007/s10008-023-05639-y.

Acknowledgements The authors extend their thanks to the Researchers Supporting Project (ref: RSPD2023R670), King Saud University, Riyadh, Saudi Arabia.

References

1. Ahmad K, Ansari SN, Natarajan K, Mobin SM (2019) A two-step modified deposition method based $(CH_3NH_3)_3Bi_2I_9$ perovskite: lead free, highly stable and enhanced photovoltaic performance. ChemElectroChem 6:1–8
2. Yue G, Lin JY, Tai SY, Xiao Y, Wu J (2012) A catalytic composite film of MoS_2/graphene flake as a counter electrode for Pt-free dye-sensitized solar cells. Electrochim Acta 85:162–168
3. Ahmad K, Song G, Kim H (2022) Fabrication of tungsten oxide/graphene quantum dot (WO_3@GQD) thin films on indium tin oxide-based glass and flexible substrates for the construction of electrochromic devices for smart window applications. ACS Sustain Chem Eng 10:11948–11957
4. Wang X, Zhao B, Kan W, Xie Y, Pan K (2022) Review on low-cost counter electrode materials for dye-sensitized solar cells: effective strategy to improve photovoltaic performance. Adv Mater Interfaces 9:2101229
5. Ahmad K, Shinde MA, Song G, Kim H (2021) Design and fabrication of $MoSe_2$/WO_3 thin films for the construction of electrochromic devices on indium tin oxide based glass and flexible substrates. Ceram Int 47:34297–34306
6. Wang H, Hu YH (2012) Graphene as a counter electrode material for dye-sensitized solar cells. Energy Environ Sci 5:8182–8188
7. Kumar P, Ahmad K, Dagar J, Unger E, Mobin SM (2021) Two-step deposition approach for lead free $(NH_4)_3Sb_2I_9$ perovskite solar cells with enhanced open circuit voltage and performance. ChemElectroChem 8:3150–3154
8. Ahmad K, Kumar P, Kim H, Mobin SM (2022) Optoelectronic and photovoltaic properties of $(NH_4)_3Bi_2I_9$: a perovskite-like energy material for Pb-free perovskite solar cells. ChemNanoMat 8:e202200061
9. Ahmad K, Khan MQ, Kim H (2022) Simulation and fabrication of all-inorganic antimony halide perovskite-like material based Pb-free perovskite solar cells. Opt Mater 128:112374
10. Ahmad K, Shinde MA, Kim H (2021) Molybdenum disulfide/reduced graphene oxide: progress in synthesis and electrocatalytic properties for electrochemical sensing and dye sensitized solar cells. Microchemical J 169:106583
11. Ahmad K, Kim H (2022) Enhanced stability of $MAPbI_3$ based perovskite solar cells. Mater Lett 318:132187
12. Ahmad K, Khan MQ, Khan RA, Kim H (2022) Numerical simulation and fabrication of Pb-free perovskite solar cells (FTO/TiO_2/$Cs_3Bi_2I_9$/spiro-MeOTAD/Au). Opt Mater 128:112458
13. Ahmad K (2020) Bismuth halide perovskites for photovoltaic applications. In: Bismuth—fundamentals and optoelectronic applications. IntechOpen, London, UK
14. Mehmood U, Malik MI, Khan AH, Hussein IA, Harrabi K, Al-Ahmed A (2018) Effect of outdoor temperature on the power-conversion efficiency of newly synthesized organic photosensitizer based dye-sensitized solar cells. Mater Lett 220:222–225
15. Robinson K, Kumara GRA, Kumara RJGLR, Jayaweera EN, Rajapakse RMG (2018) SnO_2/ZnO composite dye-sensitized solar cells with graphene-based counter electrodes. Organ Electron 56:159–162
16. Hosseinnezhad M, Rouhani S, Gharanjig K (2018) Extraction and application of natural pigments for fabrication of green dye-sensitized solar cells. Opto-Electron Rev 26:165–171
17. Chen T, Shang Y, Hao S, Tian L, Hou Y, Yang C (2018) Enhancement of dye sensitized solar cell efficiency through introducing concurrent upconversion/downconversion core/shell nanoparticles as spectral converters. Electrochim Acta 282:743–749
18. Mehrabian M, Dalir S (2018) Numerical simulation of highly efficient dye sensitized solar cell by replacing the liquid electrolyte with a semiconductor solid layer. Optik 169:214–223
19. Chen YC, Li YJ, Hsu YK (2018) Enhanced performance of ZnO-based dye-sensitized solar cells by glucose treatment. J Alloys Comp 748:382–389
20. Huaulmé Q, Cabau L, Demadrille R (2018) An important step toward more efficient and stable dye-sensitized solar cells. Chem 4:2267–2268
21. Iqbal MZ, Khan S (2018) Progress in the performance of dye sensitized solar cells by incorporating cost effective counter electrodes. Sol Energy 160:130–152
22. Atli A, Atilgan A, Yildiz A (2018) Multi-layered TiO_2 photoanodes from different precursors of nanocrystals for dye-sensitized solar cells. Sol Energy 173:752–758
23. Kumar R, Bhargava P (2018) Synthesis and characterization of carbon based counter electrode for dye sensitized solar cells (DSSCs) using organic precursor 2–2′Bipyridine (Bpy) as a carbon material. J Alloys Comp 748:905–910
24. Paymozd F, Modarresi-Alam AR, Saravani H (2022) Synthesis and characterization of chiral nano-poly [(±)-2-sec-butyl aniline] and its application in the first chiral polymer solar cell. Opt Mater 125:112098
25. Singh M, Singh D, Pal P, Singh S, Singh D, Giri BS (2023) Synthesis and performance evaluation of Beta vulgaris based

dye-sensitized organic solar cell. Environ Technol Innov 103220. https://doi.org/10.1016/j.eti.2023.103220
26. Tarique WB, Uddin A (2023) A review of progress and challenges in the research developments on organic solar cells. Mater Sci Semicond Process 163:107541
27. Bashir R, Bilal MK, Bashir A, Ali A (2023) Fabrication of PbSe colloidal quantum dot solar cells using low-temperature Li-doped ZnO electron transport layer. Sol Energy 256:67–75
28. Wang J, Peng Z, Huang J, Zhang Y, Zhang X, Wang Y, Fu Y, Li W, Chen J, Chen K (2023) Enhanced charge generation and transfer properties on anatase nanodendrite array photo-electrodes for high-efficiency quantum dot sensitized solar cells. Sol Energy Mater Sol Cells 257:112348
29. Khan U, Rauf A, Feng S, Akbar AR, Peng G, Zheng Q, Wu R, Khan M, Peng Z, Liu F (2023) Thermally stable and efficient CsF-doped all-inorganic CsPbIBr2 perovskite solar cells exceeding 15% PCE. Inorg Chem Commun 153:110862
30. Talebi H, Emami F (2023) High performance ultra-thin perovskite solar cell by surface plasmon polaritons and waveguide modes. Opti Laser Technol 165:109552
31. Song T, Zhang Z, Zhao B, Wang L, Kan W, Sun L, Wang X (2022) Boosting catalytic performance of hierarchical Co/Co0.85Se microspheres via Mott-Schottky effect toward triiodide reduction and alkaline hydrogen evolution. J Alloys Compd 918:165608
32. Liu Z, Xin W, Xie W, Wang X, Li N, Yuan Z, Li Y, Wang J (2022) Integration of hierarchical tin sulfide@sulfur-doped carbon porous composites with enhanced performance for triiodide reduction. Dyes Pigm 204:110458
33. Ahmad K, Mohammad A, Mobin SM (2017) Hydrothermally grown α-MnO_2 nanorods as highly efficient low cost counter-electrode material for dye-sensitized solar cells and electrochemical sensing applications. Electrochim Acta 252:549–557
34. Wroblowa HS, Saunders A (1973) Flow-through electrodes: II. The I^-_3/I^- redox couple. Electroanal Chem Int Electrochem 42:329–346
35. Kay A, Gratzel M (1996) Low cost photovoltaic modules based on dye sensitized nanocrystalline titanium dioxide and carbon powder. Sol Energy Mater Sol Cells 144:99–117
36. Mirzaei M, Gholivand MB (2022) Synthesis of ruthenium sulfide nanoparticles decorated on reduced graphene oxide/multi-walled carbon nanotubes as a catalytic counter electrode for dye-sensitized solar cells exceeding 13% efficiency. Sol Energy 242:212–224
37. Akman E, Karapinar HS (2022) Electrochemically stable, cost-effective and facile produced selenium@activated carbon composite counter electrodes for dye-sensitized solar cells. Sol Energy 234:368–376
38. Suzuki K, Yamaguchi M, Kumagai M, Yanagida S (2003) Application of carbon nanotubes to counter electrodes of dye-sensitized solar cells. Chem Lett 32:28–29
39. Zhang DW, Li XD, Chen S, Tao F, Sun Z, Yin XJ, Huang SM (2010) Fabrication of double-walled carbon nanotube counter electrodes for dye-sensitized solar sells. J Solid State Electrochem 14:1541–1546
40. Novoselov KS, Geim AK, Morozov SV, Jiang D, Katsnelson MI, Grigorieva IV et al (2005) Two-dimensional gas massless dirac fermions in graphene. Nature 438:197–200
41. Geim AK (2009) Graphene: status and prospects. Science 324:1530–1534
42. Castro Neto AH, Guinea F, Peres NMR, Novoselov KS, Geim AK (2009) The electronic properties of graphene. Rev Mod Phys 81:109–162
43. Zhang DW, Li XD, Li HB, Chen S, Sun Z, Yin XJ, Huang SM (2011) Graphene-based counter electrode for dye-sensitized solar cells. Carbon 49:5382–5388
44. Bonaccorso F, Sun Z, Hasan T, Ferrari AC (2010) Graphene photonics and optoelectronics. Nat Photonics 4:611–622
45. Bae S, Kim H, Lee YB, Xu XF, Park JS, Zheng Y (2010) Roll-to roll production of 30-inch graphene films for transparent electrodes. Nat Nanotechnol 5:574–578
46. Wang X, Zhi L, Tsao N, Tomović Ž, Li J, Müllen K (2008) Transparent carbon films as electrodes in organic solar cells. Angew Chem Int Ed 47:2990–2992
47. Di CA, Wei D, Yu G, Liu Y, Guo Y, Zhu D (2008) Patterned graphene as source/drain electrodes for bottom-contact organic field-effect transistors. Adv Mater 20:3289–3293
48. Schedin F, Geim AK, Morozov SV, Hill EW, Blake P, Katsnelson MI et al (2007) Detection of individual gas molecules adsorbed on graphene. Nat Mater 6:652–655
49. Lee YH, Chou A, Yu J, Chen Y, Gooding JJ (2005) Demonstration of the advantages of using bamboo-like nanotubes for electrochemical biosensor applications compared with single walled carbon nanotubes. Electrochem Commun 7:1457–1462
50. Zhou M, He J, Wang L, Zhao S, Wang Q, Cui S, Qin X, Wang R (2018) Synthesis of carbonized-cellulose nanowhisker/FeS_2@reduced graphene oxide composite for highly efficient counter electrodes in dye-sensitized solar cells. Sol Energy 166:71–79
51. Tasdemir A, Kopuklu BB, Kirlioglu AC, Gursel SA, Yurum A (2021) The influence of nitrogen doping on reduced graphene oxide as highly cyclable Li-ion battery anode with enhanced performance. Int J Hydrogen Energy 46:11865–11877
52. Wang G, Zhuo S, Xing W (2012) Graphene/polyaniline nanocomposite as counter electrode of dye-sensitized solar cells. Mater Lett 69:27–29
53. Lee KS, Lee Y, Lee JY, Ahn JH, Park JH (2012) Flexible and platinum-free dye-sensitized solar cells with conducting-polymer-coated graphene counter electrodes. Chemsuschem 5:379–382
54. Hong W, Xu Y, Lu G, Li C, Shi G (2008) Transparent graphene/PEDOT-PSS composite films as counter electrodes of dye-sensitized solar cells. Electrochem Commun 10:1555–1558
55. Choi H, Kim H, Hwang S, Choi W, Jeon M (2011) Dye-sensitized solar cells using graphene-based carbon nano composite as counter electrode. Sol Energy mater Sol Cells 95:323–325
56. Zhu G, Pan L, Lu T, Xu T, Sun Z (2011) Electrophoretic deposition of reduced graphene-carbon nanotubes composite films as counter electrodes of dye-sensitized solar cells. J Mater Chem 21:14869–14875
57. Dou YY, Li GR, Song J, Gao XP (2012) Nickel phosphide-embedded graphene as counter electrode for dye-sensitized solar cells. Phys Chem Chem Phys 14:1339–1342
58. Hou S, Cai X, Wu H, Yu X, Peng M, Yan K, Zou D (2013) Nitrogen-doped graphene for dye-sensitized solar cells and the role of nitrogen states in triiodide reduction. Energy Environ Sci 6:3356–3362
59. Wang G, Fang Y, Lin Y, Xing W, Zhuo S (2012) Nitrogen-doped graphene as transparent counter electrode for efficient dye-sensitized solar cells. Mater Res Bull 47:4252–4256
60. Xue Y, Liu J, Chen H, Wang R, Li D, Qu J, Dai L (2012) Nitrogen-doped graphene foams as metal-free counter electrodes in high-performance dye-sensitized solar cells. Angew Chem Int Ed 51:12124–12127
61. Salleh SA, Rahman MYA, Aziz THT (2022) Dye-sensitized solar cell using nickel sulfide-reduced graphene oxide counter electrode: effect of sulphur content. Inorg Chem Commun 135:109086